

Article

Comprehensive Calibration of Strap-Down Tri-Axis Accelerometer Unit

Xi Zhang ^{1,2}, Jie Li ^{1,3,*}, Li Qin ^{1,3} and Chong Shen ^{3,4}

¹ National Key Laboratory for Electronic Measurement Technology, North University of China, Taiyuan 030051, China; zhangxi@nuc.edu.cn (X.Z.); qinli@nuc.edu.cn (L.Q.)

² School of Computer Science and Control Engineering, North University of China, Taiyuan 030051, China

³ School of Instrument and Electronics, North University of China, Taiyuan 030051, China; shenchong@nuc.edu.cn

⁴ Key Laboratory of Instrumentation Science & Dynamic Measurement, Ministry of Education, North University of China, Taiyuan 030051, China

* Correspondence: lijie@nuc.edu.cn; Tel.: +86-351-355-8098

Academic Editor: Ha Duong Ngo

Received: 6 December 2016; Accepted: 21 February 2017; Published: 27 February 2017

Abstract: This paper proposes a comprehensive calibration method to improve the precision of a strap-down tri-axis accelerometer unit, in which parameters are divided into static and dynamic ones. The contribution of the manuscript is that it solves the problem of inappropriate installation and the size effect error for tri-axis accelerometer unit at high speed by using static and dynamic calibration method, respectively. The experiment results show the measuring accuracy of accelerometers is increased by more than one order of magnitude, and the navigation precision is increased by more than two orders of magnitude.

Keywords: strap-down tri-axis accelerometer; static error; dynamic error; calibration

1. Introduction

For strap-down Inertial Navigation System (SINS), an inertial measurement unit (IMU) is directly installed in the vehicle. Thus, the navigation precision of SINS depends on the measuring accuracy of IMU [1–6]. In practical application, installation of accelerometer and gyro is not orthogonal completely, and the installation error will arise. Take IMU as a rigid body. If we calibrate the orthogonal error correctly, the angular velocity can be measured regardless of position and orientation of the gyro. However, the different positions in IMU have different accelerations when it rotates. This phenomenon is the so-called size effect error or the lever arm effect error for accelerometer, which is caused by the installation position error of IMU.

Now, the existing calibration methods generally use a static model to compensate errors of the strap-down tri-axis accelerometer unit [7–21]. A multi-position calibration method was designed for microelectromechanical systems (MEMS) of high to medium quality, and the excellent performance of the proposed method was proved by experimental results [8,9]. Methods were presented to calibrate and compensate for non-zero biases, non-unit scale factors, axis misalignments and cross-axis sensitivities of both the tri-axial accelerometer and gyroscopic setups in a MEMS based IMU, which depended on the Earth's gravity as a stable physical calibration standard. In addition, experimental results showed that, with calibration, the observed average static angular error is less than a quarter of a degree and the dynamic angular error is reduced effectively [9]. An optical calibration method to address the alignment problem was proposed, and the experiments were performed with a MEMS-based azimuth-level detector to show the effectiveness of the proposed method [6]. Under the low dynamic environment, the size effect error is relatively small and can be ignored, and the above

methods are effective. However, the effect of the size error becomes serious at high angular velocity, and the navigation error caused by it should not be neglected. Therefore, we need to explore a more accurate calibration method.

In this paper, we propose a comprehensive calibration method. In this method, we assume that the position in which the specific force load on the accelerometer unit is a point, and hence a new model of dynamic error calibration is set up based on this method. The proposed method includes 15 parameters. In the parameters, there are three zero bias voltages, nine installation angles and three related factors, respectively. The errors of the accelerometer are completely separated through calibration of 15 parameters, which can fully reflect the characteristics of the sensor itself and improve measurement accuracy of the sensor. The proposed method makes the coordinate system of the accelerometer correspondent to the standard orthogonal coordinate system of carrier. After calibration, it can make three installation directions of the accelerometer completely equivalent to the standard coordinate system and ensure the accelerometer unit better perpendicularity.

A list of nomenclature is given as follows:

- (1) SINS: strap-down inertial navigation system;
- (2) IMU: inertial measurement unit;
- (3) MIMU: MEMS inertial measurement unit.

2. Calibration Model

Accuracy of the calibration is the premise of compensating of tri-accelerometer unit. Here, we define the coordinate system as the following:

- (1) Body coordinate frame (b-frame): its origin O_b is the center of IMU, three orthogonal axials are represented as x_b, y_b and z_b , respectively, and $(r_x r_y r_z)$ is the distance between position of the accelerometer and origin O , respectively.
- (2) Sensitive axis coordinate frame (a-frame): x_a, y_a and z_a represent a three-coordinate axis in an a-frame.
- (3) Navigation coordinate system (n-frame): its origin O is at the center of the gravity vector.

2.1. Calibration Model of Static Error

In this paper, the installation position error is defined as the relative location between the actual sensitive spot of each accelerometer and the coordinate origin of the IMU structure. In order to reduce the output error, the installation errors should be compensated, and the accelerometer output should be transformed from a-frame to b-frame. The coordinate systems mentioned above are shown in Figure 1.

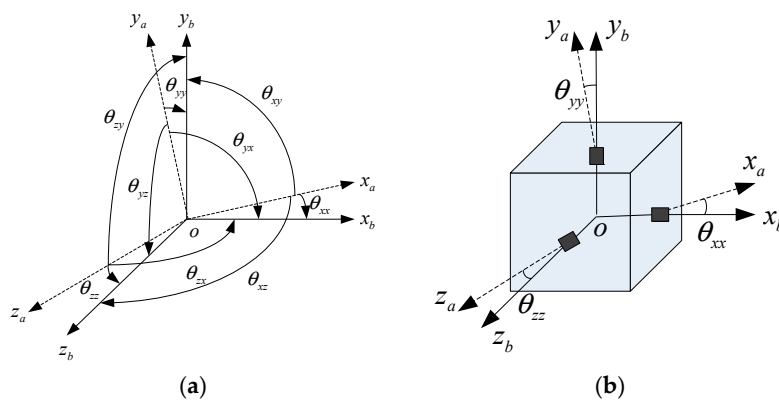


Figure 1. Model of static calibrate for accelerometer unit: (a) angles between a-frame and b-frame; (b) installation of tri-accelerometer unit.

Figure 1 represents the hexahedral reference orthogonal coordinate system $O_b x_b y_b z_b$ of MIMU, and the non-orthogonal coordinate system, which is the actual measuring direction for accelerometers. For simplicity, O_b and O_a are set at the same point O .

In Figure 1, $\theta_{xx}, \theta_{xy}, \theta_{xz}, \theta_{yx}, \theta_{yy}, \theta_{yz}, \theta_{zx}, \theta_{zy}$ and θ_{zz} are installation angles for tri-accelerometers unit, and θ_{ij} is the angle between a_i and b_j .

k_x^a, k_y^a and k_z^a are scale factors of three accelerometers. u_{x0}^a, u_{y0}^a , and u_{z0}^a are zero bias voltage. x_b, y_b , and z_b are three axial directions of reference frame, f_x^b, f_y^b , and f_z^b are a specific force in reference frame b, x_a, y_a , and z_a are actual axial directions, and f_x^a, f_y^a , and f_z^a are a specific force in reference frame a.

The output u_i^a of A_i in a-frame can be given in Equation (1)

$$u_i^a = k_i^a f_i^a + u_{i0}^a + \delta_i = k_i^a (f_i^a + B_i^a) + \delta_i, (i = x, y, z) \tag{1}$$

Here, $u_{i0}^a = k_i^a \cdot B_i^a$, $B_i^a = \frac{u_{i0}^a}{k_i^a}$, $u_i^a, k_i^a, B_i^a, f_i^a$ are output voltage, scale factors, zero bias, and actual specific force input, respectively. The noise error δ_i can be ignored. Equation (1) can be simplified as:

$$u_i^a = k_i^a f_i^a + u_{i0}^a = k_i^a (f_i^a + B_i^a), (i = x, y, z) \tag{2}$$

If we set C_a^b as a transition matrix from a to b reference frame, specific forces can be changed from an a to b reference frame followed by $f^b = C_a^b f^a$, namely

$$f^b = \begin{bmatrix} f_x^b \\ f_y^b \\ f_z^b \end{bmatrix} = \begin{bmatrix} C_a^b(1,1) & C_a^b(1,2) & C_a^b(1,3) \\ C_a^b(2,1) & C_a^b(2,2) & C_a^b(2,3) \\ C_a^b(3,1) & C_a^b(3,2) & C_a^b(3,3) \end{bmatrix} \begin{bmatrix} f_x^a \\ f_y^a \\ f_z^a \end{bmatrix} = C_a^b f^a \tag{3}$$

Because the reference frame b is orthogonal, and C_a^b is an orthogonal matrix, f^a can be given by

$$f^a = C_a^b f^b = (C_a^b)^{-1} f^b = (C_a^b)^T f^b \\ = \begin{bmatrix} C_a^b(1,1) & C_a^b(2,1) & C_a^b(3,1) \\ C_a^b(1,2) & C_a^b(2,2) & C_a^b(3,2) \\ C_a^b(1,3) & C_a^b(2,3) & C_a^b(3,3) \end{bmatrix} \begin{bmatrix} f_x^b \\ f_y^b \\ f_z^b \end{bmatrix} \tag{4}$$

Substituting Equation (4) into Equation (2), u_i^a is simplified as Equation (5)

$$u_i^a = \begin{bmatrix} u_x^a \\ u_y^a \\ u_z^a \end{bmatrix} = \begin{bmatrix} k_x & 0 & 0 \\ 0 & k_y & 0 \\ 0 & 0 & k_z \end{bmatrix} \begin{bmatrix} f_x^a \\ f_y^a \\ f_z^a \end{bmatrix} + \begin{bmatrix} u_{x0}^a \\ u_{y0}^a \\ u_{z0}^a \end{bmatrix} = K (C_a^b)^T f^b + u_{i0}^a \tag{5}$$

From Equation (5), f^b are obtained in Equation (6)

$$f^b = [K \cdot (C_a^b)^T]^{-1} (u_i^a - u_{i0}^a) \\ = [(C_a^b)^T]^{-1} [K^{-1} (u_i^a - u_{i0}^a)] = K_A \cdot U_A - \nabla^b \tag{6}$$

Because $U_A = (u_x^a \ u_y^a \ u_z^a)^T$ are the results from three accelerometers, K_A is scale factor, and K_A^{-1} is given by Equation (7)

$$K_A^{-1} = K \cdot (C_a^b)^T \\ = \begin{bmatrix} k_x C_a^b(1,1) & k_x C_a^b(2,1) & k_x C_a^b(3,1) \\ k_y C_a^b(1,2) & k_y C_a^b(2,2) & k_y C_a^b(3,2) \\ k_z C_a^b(1,3) & k_z C_a^b(2,3) & k_z C_a^b(3,3) \end{bmatrix} \tag{7}$$

$\mathbf{B} = \left(B_x^a \ B_y^a \ B_z^a \right)^T$ is a vector of zero bias specific force, and then the equivalent zero bias vector ∇^b is given by Equation (8):

$$\begin{aligned} \nabla^b &= \left[(\mathbf{C}_a^b)^T \right]^{-1} \left[(\mathbf{K})^{-1} \mathbf{u}_{i0}^a \right] \\ &= \left[(\mathbf{C}_a^b)^T \right]^{-1} \left[(\mathbf{K})^{-1} k_i^a \mathbf{B}_i^a \right] = \left[(\mathbf{C}_a^b)^T \right]^{-1} \mathbf{B} \end{aligned} \tag{8}$$

$\mathbf{C}_a^b(*, j)$ is the unit column vector of the conversion matrix, and its element value is the direction cosine of A_j and the unit vectors $\mathbf{i}_x^b, \mathbf{i}_y^b, \mathbf{i}_z^b$, that is, Equation (9):

$$\mathbf{C}_a^b(*, j) = \begin{bmatrix} \cos \theta_{xx} & \cos \theta_{yx} & \cos \theta_{zx} \\ \cos \theta_{xy} & \cos \theta_{yy} & \cos \theta_{zy} \\ \cos \theta_{xz} & \cos \theta_{yz} & \cos \theta_{zz} \end{bmatrix} \tag{9}$$

The results of $\mathbf{K}, \mathbf{C}_a^b, \mathbf{u}_{i0}, \mathbf{B}_{i0}$ and \mathbf{f}^b , which are known from Equations (6), (8) and (9) can be obtained by using multi-position static turntable calibration tests.

Measurement reference point of specific force \mathbf{f}^b should be at a b coordinate origin. However, the static calibration can only determine the direction of accelerometer and can not determine the actual sensitive point. Therefore, the dynamic calibration is necessary during measurement.

2.2. Calibration Model of Dynamic Error

Linear velocity of any point in rigid body is $v = \omega \times r$, as shown in Figure 2, a is the acceleration of some point, and then:

$$\begin{aligned} a &= \frac{dv}{dt} = \frac{d(\omega \times r)}{dt} \\ &= \frac{d\omega}{dt} \times r + \omega \times \frac{dr}{dt} = \dot{\omega} \times r + \omega \times v \\ &= \dot{\omega} \times r + \omega \times (\omega \times r) = a_t + a_n \end{aligned} \tag{10}$$

a_t is tangential acceleration, and a_n is normal acceleration. MIMU is regarded as a rigid body. The acceleration of each point in the rigid body is different when the angular motion happens. The measurement point of the specific force is different from the existence of installation position error. It is necessary to compensate the dynamic error and make the measurement point equivalent to a point.

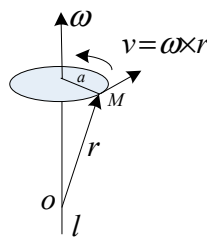


Figure 2. Diagram of dynamic error caused by the size effect.

In Figure 3, accelerometer A_x is taken as an example. A_x is the sensitive point of an accelerometer, the frame $Ox_b y_b z_b$ is the calibration coordinate system (frame b), and point O is the reference point of the sensitive value. Installation position or sensitive direction of A_x is $\mathbf{C}_a^b(*, 1)$. \mathbf{r}_1^b is the position vector from A_x point to the origin of frame b.

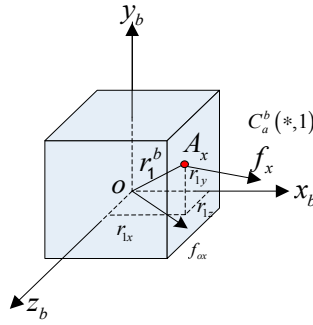


Figure 3. Model of dynamic calibrate for accelerometer A_x .

Specific force at point A_x is f_x , and specific force at point O is f_{ox} . When there is an angular motion, we can get the relationship between two specific forces in Equation (11)

$$\begin{aligned} f_x^b &= f_{ox}^b + \dot{\omega}^b \times r_1^b + \omega^b \times (\omega^b \times r_1^b) \\ &= f_{ox}^b + \left[\dot{\omega}^b \times + (\omega^b \times)^2 \right] r_1^b = f_{ox}^b + W r_1^b \end{aligned} \tag{11}$$

$W = \left(\dot{\omega}^b \times \right) + (\omega^b \times)^2$, ω is angular velocity, $\dot{\omega}^b \times r_1^b$, and $\omega^b \times (\omega^b \times r_1^b)$ are tangential acceleration and normal acceleration. $(\bullet \times)$ is an anti-symmetric matrix that is formed by a vector, and $(\omega^b \times)^2$ is a symmetric matrix. The projections of installation position r_x^b in frame b are r_{1x}^b , r_{1y}^b and r_{1z}^b , Equation (11) is projected to the x -axis in frame a , that is, multiply $C_a^b(*,1)^T$ to both sides of Equation (12), and the specific force output of x -axis can be obtained:

$$f_X = C_a^b(*,1)^T f_x^b = C_a^b(*,1)^T f_{ox}^b + C_a^b(*,1)^T W r_1^b = f_{oX} + f_{XL} \tag{12}$$

f_X is the specific force along the sensitive axis of sensor, f_{oX} is the projection that is sensitive to specific force in frame b , and f_{XL} is the specific force error caused by lever arm effect. Then, Equation (13) can be obtained:

$$u_X = k_X(B_X + f_X) = k_X(B_X + f_{oX}^a + f_{XL}) \tag{13}$$

Similarly, the deduction of y -axis and z -axis can be obtained:

$$\begin{bmatrix} u_X \\ u_Y \\ u_Z \end{bmatrix} = \begin{bmatrix} k_X & 0 & 0 \\ 0 & k_Y & 0 \\ 0 & 0 & k_Z \end{bmatrix} \cdot \left(\begin{bmatrix} B_X \\ B_Y \\ B_Z \end{bmatrix} + \begin{bmatrix} f_{oX}^a \\ f_{oY}^a \\ f_{oZ}^a \end{bmatrix} + \begin{bmatrix} f_{XL} \\ f_{YL} \\ f_{ZL} \end{bmatrix} \right) \tag{14}$$

Equation (14) can be simplified as

$$U_A = K(B + f_o^a + f_L) \tag{15}$$

According to static calibration model $f^a = (C_a^b)^T f^b$, we can obtain $U_A = K[B + (C_a^b)^T f^b + f_L]$. Then,

$$f^b = \left[(C_a^b)^T \right]^{-1} \left[U_A(K)^{-1} - B - f_L \right] = K_A \cdot U_A - \nabla^b - f_L^b \tag{16}$$

$f_L^b = \left[(C_a^b)^T \right]^{-1} f_L$ is the acceleration compensation of dynamic calibration and is composed of direction matrix C_a^b , angle rate ω^b and installation position vector r^b , namely, dynamic calibration added the f_L^b compared with static position. We have:

$$\mathbf{f}_L^b = \left[\left(\mathbf{C}_a^b \right)^T \right]^{-1} \begin{bmatrix} \mathbf{C}_a^b(*,1)^T W r_X^b \\ \mathbf{C}_a^b(*,2)^T W r_Y^b \\ \mathbf{C}_a^b(*,3)^T W r_Z^b \end{bmatrix} \tag{17}$$

When ω is a constant value, $\dot{\omega} = 0$, W is simplified as $W = (\omega \times)^2$.

2.3. Identification of Lever Arm

Installed direction error has been compensated by using the static calibration. Sensing axes of the three accelerometers are perpendicular orthogonal, which are parallel to the carrier frame, respectively.

When accelerometers rotate at a constant speed of ω_0 ($\dot{\omega}_0 = 0$), installation vector is $\mathbf{r}_i^b = (r_{ix} \ r_{iy} \ r_{iz})$, for which $i = 1,2,3$ is the number of accelerometer. r_x, r_y, r_z are vectors along three axes, respectively. As sensing direction of A_i is along the input axis, and the error caused by the lever arm is $\omega \times (\omega \times r)$ on frame b. In order to identify parameter r easily, the following method is used.

If we set $\mathbf{f}_{i0}^{xb} = (g \ 0 \ 0)$ and $\mathbf{r}_1 = (r_{1x} \ r_{1y} \ r_{1z})$, then the output of the three accelerometers are given by:

$$\begin{cases} \mathbf{f}_{x0}^{xa} = \mathbf{C}_a^b(*,1)^T \mathbf{f}_0^{xb}, i = x, y, z \\ \mathbf{f}_{y0}^{xa} = \mathbf{C}_a^b(*,2)^T \mathbf{f}_0^{xb}, i = x, y, z \\ \mathbf{f}_{z0}^{xa} = \mathbf{C}_a^b(*,3)^T \mathbf{f}_0^{xb}, i = x, y, z \end{cases} \tag{18}$$

$$\begin{cases} f_{x0}^{xa} = \begin{pmatrix} \cos \theta_{xx} & \cos \theta_{xy} & \cos \theta_{xz} \end{pmatrix} \begin{pmatrix} f_{x0}^{xb} & f_{y0}^{xb} & f_{z0}^{xb} \end{pmatrix}^T \\ f_{y0}^{xa} = \begin{pmatrix} \cos \theta_{yx} & \cos \theta_{yy} & \cos \theta_{yz} \end{pmatrix} \begin{pmatrix} f_{x0}^{xb} & f_{y0}^{xb} & f_{z0}^{xb} \end{pmatrix}^T \\ f_{z0}^{xa} = \begin{pmatrix} \cos \theta_{zx} & \cos \theta_{zy} & \cos \theta_{zz} \end{pmatrix} \begin{pmatrix} f_{x0}^{xb} & f_{y0}^{xb} & f_{z0}^{xb} \end{pmatrix}^T \end{cases} \tag{19}$$

The equation above is simplified as Equation (20):

$$\mathbf{f}_{i0}^{xa} = \mathbf{C}_a^b(*,j)^T \mathbf{f}_{i0}^{xb} \tag{20}$$

Here, we define $i = x, y, z, j = 1, 2, 3$, respectively.

Similarly, $\mathbf{f}_{i0}^{yb} = (0 \ g \ 0)$, $\mathbf{f}_{i0}^{zb} = (0 \ 0 \ g)$, i.e., $\mathbf{f}_{i0}^{ya} = \mathbf{C}_a^b(*,j)^T \mathbf{f}_{i0}^{yb}$, $\mathbf{f}_{i0}^{za} = \mathbf{C}_a^b(*,j)^T \mathbf{f}_{i0}^{zb}$. Installation vector is $\mathbf{r}_j = (r_{jx} \ r_{jy} \ r_{jz})$, ($j = 1, 2, 3$).

When the x -axis is vertically upward, turntable rotation at a constant angular velocity ω_0 and specific force output in carrier frame is given by:

$$\mathbf{f}_{1i}^a = \mathbf{C}_a^b(*,j)^T \mathbf{f}_1^{xb} = \mathbf{C}_a^b(*,j)^T (\mathbf{f}_1^{xb} + \omega \times \omega \times r_i)$$

$$\begin{cases} f_x^{xa} = \begin{bmatrix} \cos \theta_{xx} & \cos \theta_{xy} & \cos \theta_{xz} \end{bmatrix} \begin{bmatrix} g & -\omega_0^2 r_{1y} & -\omega_0^2 r_{1z} \end{bmatrix}^T \\ f_y^{xa} = \begin{bmatrix} \cos \theta_{yx} & \cos \theta_{yy} & \cos \theta_{yz} \end{bmatrix} \begin{bmatrix} g & -\omega_0^2 r_{2y} & -\omega_0^2 r_{2z} \end{bmatrix}^T \\ f_z^{xa} = \begin{bmatrix} \cos \theta_{zx} & \cos \theta_{zy} & \cos \theta_{zz} \end{bmatrix} \begin{bmatrix} g & -\omega_0^2 r_{3y} & -\omega_0^2 r_{3z} \end{bmatrix}^T \end{cases} \tag{21}$$

Similarly, when the y -axis and z -axis are vertically upward on 1 g, the control turntable rotates at a constant angular velocity ω_0 and specific force outputs in the carrier frame are:

$$\begin{cases} f_x^{ya} = \begin{bmatrix} \cos \theta_{xx} & \cos \theta_{xy} & \cos \theta_{xz} \end{bmatrix} \begin{bmatrix} -\omega_0^2 r_{1x} & g & -\omega_0^2 r_{1z} \end{bmatrix}^T \\ f_y^{ya} = \begin{bmatrix} \cos \theta_{yx} & \cos \theta_{yy} & \cos \theta_{yz} \end{bmatrix} \begin{bmatrix} -\omega_0^2 r_{2x} & g & -\omega_0^2 r_{2z} \end{bmatrix}^T \\ f_z^{ya} = \begin{bmatrix} \cos \theta_{zx} & \cos \theta_{zy} & \cos \theta_{zz} \end{bmatrix} \begin{bmatrix} -\omega_0^2 r_{3x} & g & -\omega_0^2 r_{3z} \end{bmatrix}^T \end{cases} \tag{22}$$

$$\begin{cases} f_x^{za} = \begin{bmatrix} \cos \theta_{xx} & \cos \theta_{xy} & \cos \theta_{xz} \end{bmatrix} \begin{bmatrix} -\omega_0^2 r_{1x} & -\omega_0^2 r_{1y} & g \end{bmatrix}^T \\ f_y^{za} = \begin{bmatrix} \cos \theta_{yx} & \cos \theta_{yy} & \cos \theta_{yz} \end{bmatrix} \begin{bmatrix} -\omega_0^2 r_{2x} & -\omega_0^2 r_{2y} & g \end{bmatrix}^T \\ f_z^{za} = \begin{bmatrix} \cos \theta_{zx} & \cos \theta_{zy} & \cos \theta_{zz} \end{bmatrix} \begin{bmatrix} -\omega_0^2 r_{3x} & -\omega_0^2 r_{3y} & g \end{bmatrix}^T \end{cases} \quad (23)$$

According to Equation (23), installation position vectors can be given as

$$\begin{cases} r_{jx} = (f_i^{xa} - f_i^{ya} - f_i^{za} - f_{i0}^{xa} + f_{i0}^{za} + f_{i0}^{ya}) / 2\omega_0^2 \cos \theta_{ix} \\ r_{jy} = (f_i^{ya} - f_i^{xa} - f_i^{za} - f_{i0}^{ya} + f_{i0}^{za} + f_{i0}^{xa}) / 2\omega_0^2 \cos \theta_{iy} \\ r_{jz} = (f_i^{za} - f_i^{xa} - f_i^{ya} - f_{i0}^{za} + f_{i0}^{ya} + f_{i0}^{xa}) / 2\omega_0^2 \cos \theta_{iz} \end{cases}, (j = 1, i = x; j = 2, i = y; j = 3, i = z). \quad (24)$$

We can get values of r_1, r_2, r_3 if f_i^a, f_{i0}^a are given by Equation (2). In the procedure of calibration, owing to the direction cosine in the denominator approach zero, so it becomes distortion that results in the amplification of calculation error. We make an angle deviate between the turntable frame and carrier frame, and use the turntable to avoid the problems. Through numerous experiments at high speed, we can obtain mean values and also provide a more accurate calibration result for subsequent compensation.

Actually, $r = \begin{pmatrix} 0.01 & 0.01 & 0.01 \end{pmatrix}$ (unit m), according to $\delta a = \omega^2 r$, when rotating at a speed of $100^\circ/s$, the acceleration error will be 0.03 m/s^2 . If the period of the measurement takes 100 s, the velocity error will be 3 m/s, and displacement error will be 150 m. Namely, the installation position error can not be ignored.

3. Experiments

In order to verify the effectiveness of the proposed method, the static and dynamic experiments are carried out. Furthermore, a ground semi-physical experiment is developed, and the experimental results of pre- and pro- compensation are compared. In this system, the zero bias stability, repeatability, and resolution are 1 mg.

3.1. Static Calibration Experiment

- (1) MIMU, which linked with a real-time acquisition system to collect data, is fixed on the multi-function tri-axial position rate turntable. x -axis upward, y -axis and z -axis point to south and east directions, respectively.
- (2) By setting the turntable position, make accelerometer x ideal axis at position $\pm 1 \text{ g}$ and collect the output data for a minute at each position.
- (3) Turntable is set to make the accelerometers y -axis and z -axis in position $\pm 1 \text{ g}$. Collect the output data for a minute at each position.
- (4) According to static parameters calibration model Equation (6), the least squares fitting results can be obtained by using Matlab (version 7.8.0 (R2009a), MathWorks, Natick, MA, USA), which are actual installation angle, zero bias and scale factors of tri-axial accelerometers, respectively.

3.2. Dynamic Calibration Experiment

- (1) Fix the MIMU on the turntable, set up the turntable to the x -axis in the vertical position steady for two minutes.
- (2) Power on the acquisition system and collect one-minute stationary data. Then, set the turntable rate to rotate in an invariable angular rate $\omega_0 = 100^\circ/s, 150^\circ/s, \text{ and } 200^\circ/s$ around the x -axis and collect one minute of data after becoming stable.
- (3) Set the turntable to the y -axis and z -axis on the upright position, repeat the first step and record the output of tri-axial accelerometer timely.

3.3. Ground Verification Experiment

To verify the effect of the result of calibration for the navigation measurement accuracy, the ground semi-physical simulation experiment is carried out on a tri-axial rate position turntable as shown in Figure 4. Here, the simulated data is only to show the effectiveness reducing dynamic errors and the simulated data does not include all the error sources. The main equipment includes: (1) high precision three-axis position and velocity turntable; (2) tri-axis accelerometer unit; (3) data acquisition system; and (4) power supply. The type of the accelerometer is MS9005.D (Colibrys, Yverdon-les-Bains, Switzerland), the measurement range is ± 5 g, the bias stability is less than 0.75 mg, and the nonlinearity is less than 0.8%.

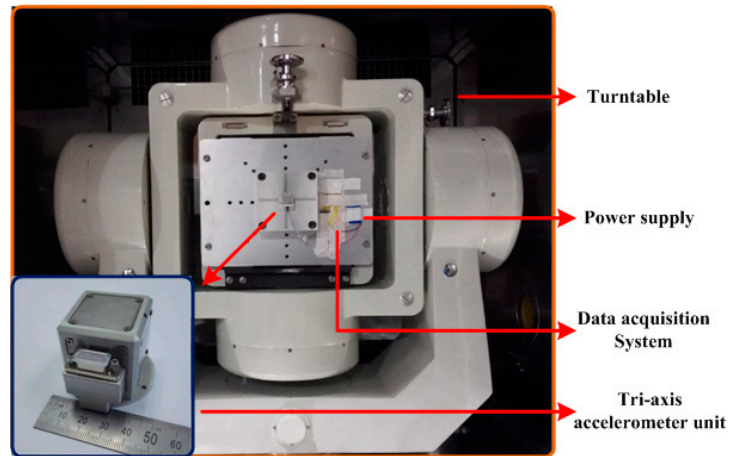


Figure 4. Ground experimental equipment.

4. Result/Discussion

4.1. Static Calibration Result and Discussion

Static and calibration results of accelerometer unit are given in Table 1. Figure 5 is a contrast of the accelerometer outputs' pre- and pro- calibration and compensation by using the proposed method. Table 2 gives the outputs of three-axis acceleration pre- and pro- compensation when the x -axis is at the ± 1 g position. The absolute error of the accelerometer outputs is less than 1 mg after compensation, and the measurement accuracy is increased by one or two magnitude.

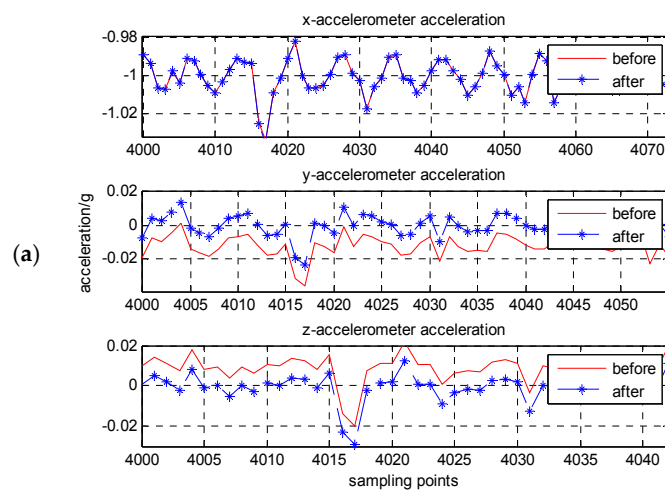


Figure 5. Cont.

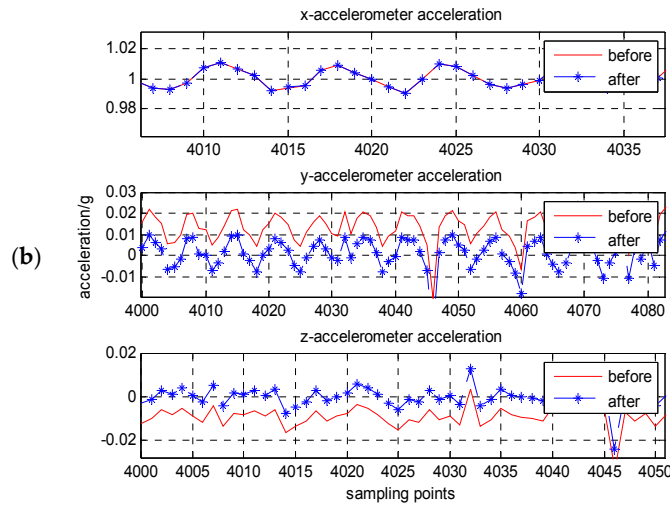


Figure 5. Contrast of three-axis acceleration before and after compensation when the x -axis, respectively, at ± 1 g position: (a) x -axis at -1 g position; (b) x -axis at $+1$ g position.

Table 1. Static calibration of accelerometer unit.

No.	Zero Bias (V)	Scale Factor (V/g)	Installation Angle (Degree)
1	2.405098	0.39496	(0.75997, 90.71425, 89.74038)
2	2.380978	0.39808	(89.25516, 0.74486, 90.5630)
3	2.435503	0.40024	(90.52202, 89.17706, 0.97456)

Table 2. Output of tri-accelerometer unit when the accelerometer of the x -axis is ± 1 g (unit: g).

Sensor	Theoretical Output	Before Compensation	After Compensation	Before Compensation	After Compensation
x	± 1 g	1.00043	1.00041	-0.99956	-0.99958
y	0 g	0.01299	0.00098	-0.01100	0.00098
z	0 g	-0.00911	0.00023	0.00953	0.00020

Navigation calculation starts with initial speed zero. Figure 6a,b are three-dimensional velocity and position information of the carrier before compensation. Figure 7a,b are three-dimensional velocity and position information of the carrier after the calibration compensation. It can be seen from the figures that the velocity error reduced from 4 to 0.02 m/s after calibration and compensation, and the position error reduced from 100 to 0.3 m.

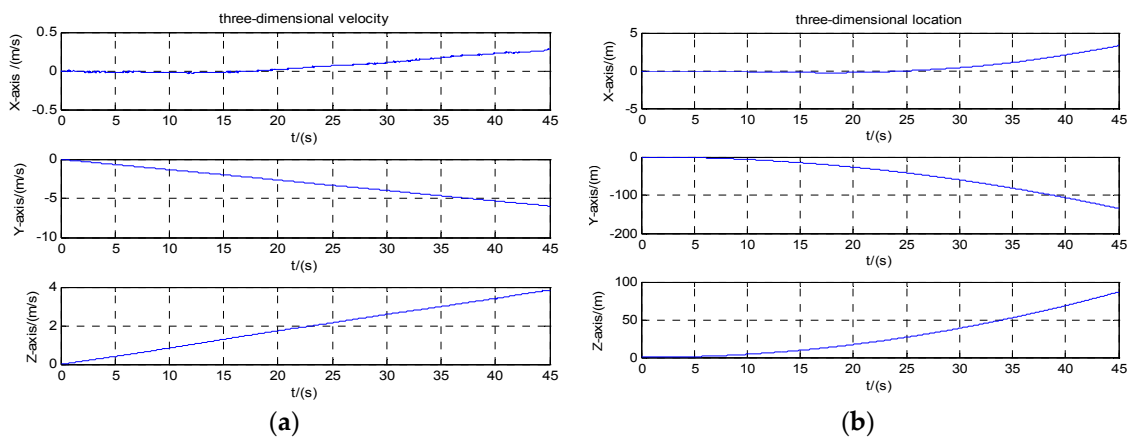


Figure 6. Velocity and position before compensation: (a) velocity; (b) position.

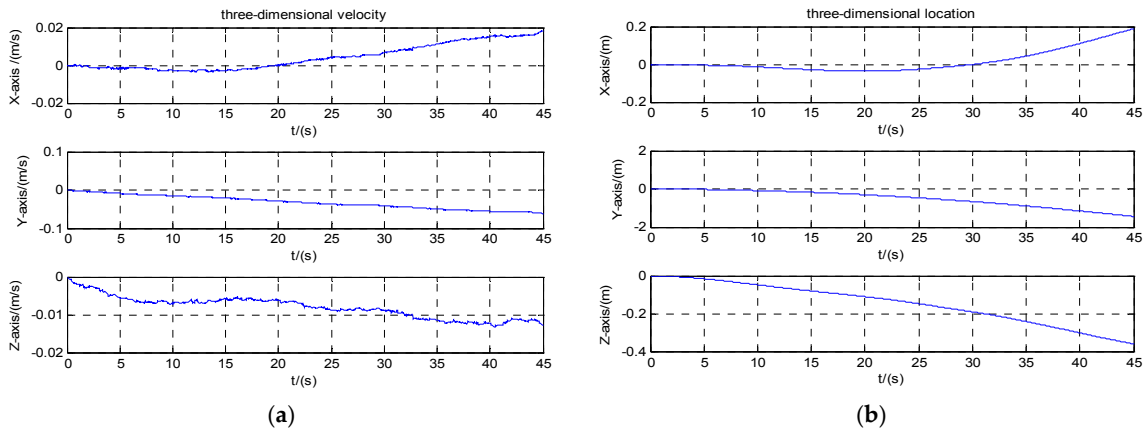


Figure 7. Velocity and position after compensation: (a) velocity; (b) position.

4.2. Dynamic Calibration Result and Discussion

Similarity to the results of static calibration described above, Figure 8 is a contrast of the accelerometer outputs' pre- and pro- calibration and compensation by using the proposed method. The result of dynamic calibration for the accelerometer unit is given in Table 3. Table 4 gives the outputs of three-axis acceleration pre- and pro- compensation when the x-axis at ± 1 g position. The absolute error of the accelerometer outputs is less than 1 mg after compensation, and the measurement accuracy is increased by one or two magnitude.

Table 3. Dynamic calibration for accelerometer unit.

Installation Position Vector	Installation Position Vector (m)		
r1	-0.00834	-0.00042	-0.00132
r2	-0.00256	-0.00893	-0.00026
r3	-0.00060	-0.00050	-0.00824

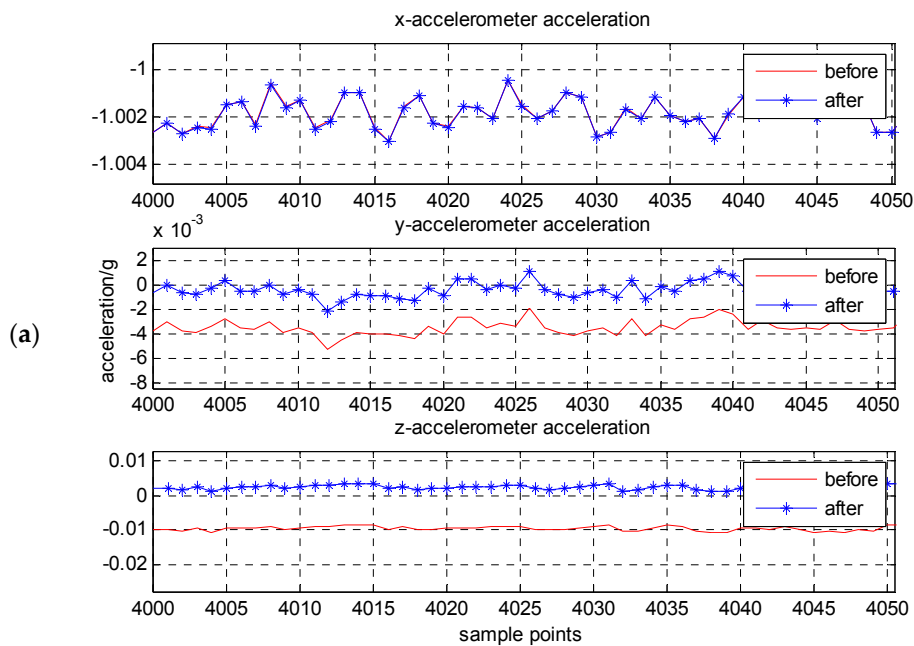


Figure 8. Cont.

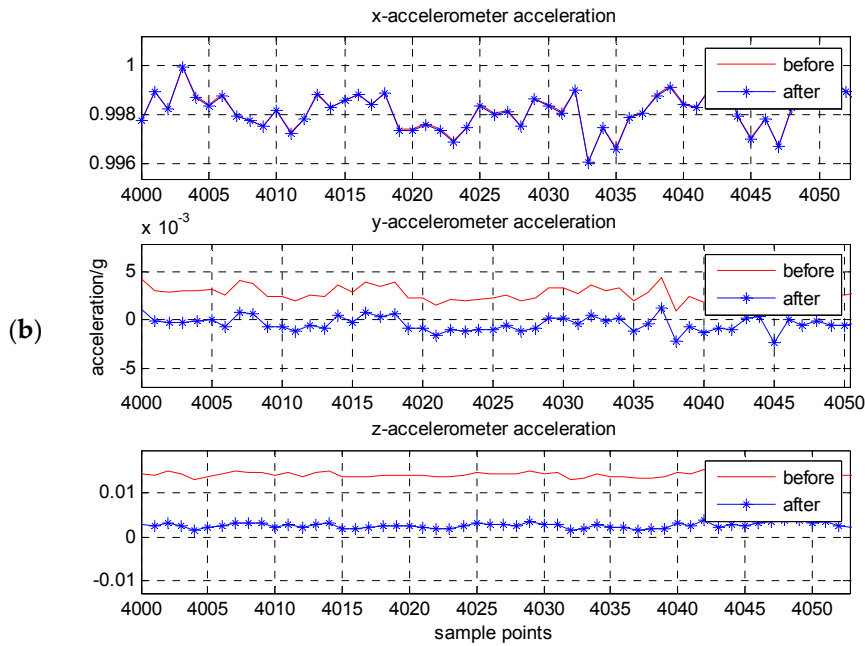


Figure 8. The contrast of three-axis acceleration before and after compensation when the x -axis, respectively, at ± 1 g position: (a) x -axis at -1 g position; (b) x -axis at $+1$ g position.

Table 4. Output of the tri-accelerometer unit when the accelerometer of the x -axis is ± 1 g. (unit: g).

Sensor	Theoretical Output	Before Compensation	After Compensation	Before Compensation	After Compensation
x	± 1 g	0.998078	0.998060	-1.001924	-1.001939
y	0 g	0.000289	0.000253	-0.003359	0.000253
z	0 g	-0.014150	0.002402	0.0093985	0.002402

To illustrate the performance of the proposed dynamic calibration method, Figures 9 and 10 depict the three-dimensional velocity and position information of the carrier before and after compensation. Because of the dynamic calibration and compensation of accelerometer, it can be seen that the system’s velocity and position error is significantly reduced.

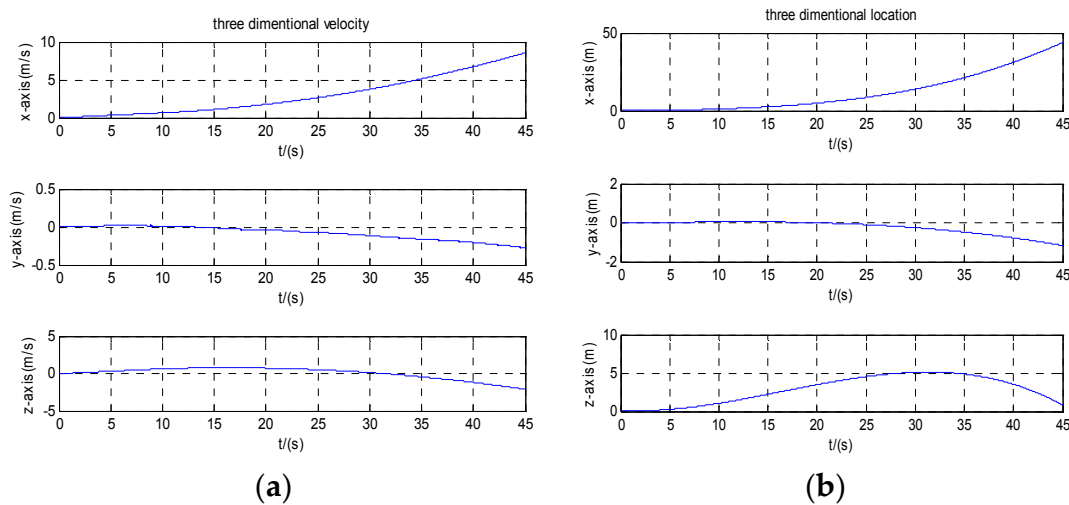


Figure 9. Velocity and position before compensation: (a) velocity; (b) position.

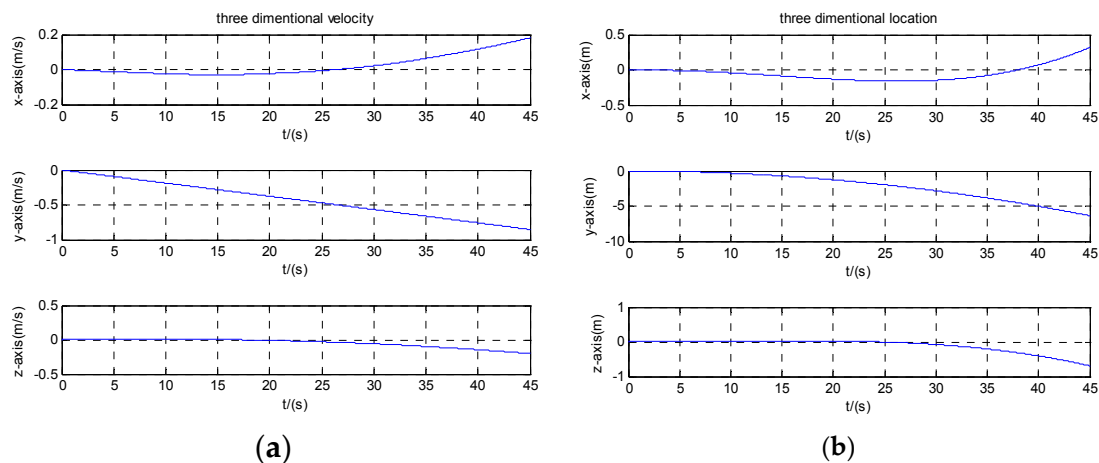


Figure 10. Velocity and position after compensation: (a) velocity; (b) position.

5. Conclusions

We developed a static and dynamic compensation method for an accelerometer unit, which can make the measuring accelerometer equivalent to a point. In this calibration method, 15 parameters for a tri-axis accelerometer unit were used. Besides the zero bias voltage, the other parameters have different physical significance in contrast with the existing calibration methods.

The proposed calibration method can effectively remove the dimension effect in dynamic environment. The turntable and semi-physical simulation experiments have to be performed to verify the validity of this dynamic method. The results show that the navigation precision of tri-axis accelerometers can be largely improved at high speed after compensation.

The future work is to reduce the inertial navigation error accumulated along with time for IMU.

Acknowledgments: We acknowledge the support from the China National Funds for Distinguished Young Scientists (No. 51225504), the National 973 Program (2012CB723404), the National Science Foundation of China (Nos. 51575500, 50905169) and the Projects Supported by Shanxi Province Outstanding Researcher (2016M180018).

Author Contributions: X.Z., J.L. and L.Q. conceived and designed the experiments; X.Z. and C.S. performed the experiments; X.Z., J.L. and C.S. analyzed the data; X.Z. and C.S. contributed reagents/materials/analysis tools; X.Z. wrote the paper.

Conflicts of Interest: The authors declare no conflict of interest.

References

1. Savage, P.G. Strapdown inertial navigation integration algorithm design part 1: Attitude algorithms. *J. Guid. Control Dyn.* **1998**, *21*, 19–28. [[CrossRef](#)]
2. Savage, P.G. Strapdown inertial navigation integration algorithm design part 2: Velocity and position algorithm. *J. Guid. Control Dyn.* **1998**, *21*, 208–221. [[CrossRef](#)]
3. Davis, B.S. Using low-cost MEMS accelerometers and gyroscopes as strapdown IMUs on rolling projectiles. In Proceedings of the IEEE Position Location & Navigation Symposium, Palm Springs, CA, USA, 20–23 April 1998; pp. 594–601.
4. Aydemir, G.A.; Saranli, A. Characterization and calibration of MEMS inertial sensors for state and parameter estimation applications. *Measurement* **2012**, *45*, 1210–1225. [[CrossRef](#)]
5. Peng, H.; Zhi, X.; Wang, R.; Liu, J.Y.; Zhang, C. A new dynamic calibration method for IMU deterministic errors of the INS on the hypersonic cruise vehicles. *Aerosp. Sci. Technol.* **2014**, *32*, 121–130. [[CrossRef](#)]
6. Zhu, R.; Zhao, Y.Z. Calibration of three-dimensional integrated sensors for improved system accuracy. *Sens. Actuators A* **2006**, *127*, 340–344. [[CrossRef](#)]
7. Yan, M.; Weng, H.N.; Xie, Y. Calibration for system parameters and scaling for installation errors of IMU. *J. Chin. Inert. Technol.* **2006**, *14*, 27–29.

8. Syed, Z.F.; Aggarwal, P.; Goodall, C.; Niu, X.; Sheimy, N. A new multi-position calibration method for MEMS inertial navigation systems. *Meas. Sci. Technol.* **2007**, *18*, 897–907. [[CrossRef](#)]
9. Fong, W.T.; Ong, S.K.; Nee, A.Y. Method for in-field use calibration of an inertial measurement unit without external equipment. *Meas. Sci. Technol.* **2008**, *19*, 32–38. [[CrossRef](#)]
10. Li, J.; Hong, H.H.; Zhang, W.D. Research on calibration techniques for MEMS-micro inertial measurement unit. *Chin. J. Sens. Act.* **2008**, *21*, 1169–1173.
11. Hwangbo, M.; Kim, J.S.; Kanade, T. IMU self-calibration using factorization. *IEEE Trans. Robot.* **2013**, *29*, 493–507. [[CrossRef](#)]
12. Li, C.; Zhang, S.F.; Cao, Y. One new onboard calibration scheme for gimbaled IMU. *Measurement* **2013**, *46*, 2359–2375. [[CrossRef](#)]
13. Zhang, X.M.; Chen, G.B.; Li, J. Calibration of triaxial MEMS vector field measurement system. *IET Sci. Meas. Technol.* **2014**, *8*, 601–609.
14. Ma, L.; Chen, W.W.; Li, B. Fast field calibration of MIMU based on the powell algorithm. *Sensors* **2014**, *14*, 16062–16081. [[CrossRef](#)] [[PubMed](#)]
15. Dar, T.; Suryanarayanan, K.; Geisberger, A. No physical stimulus testing and calibration for MEMS accelerometer. *J. Microelectromech. Syst.* **2014**, *23*, 811–818. [[CrossRef](#)]
16. Jan, R.; Martin, S.; Jakub, S. Calibration of low-cost triaxial inertial sensors. *IEEE Instrum. Meas. Mag.* **2015**, *18*, 32–38.
17. Lueken, M.; Misgeld, J.E.; Rueschen, D. Multi-sensor calibration of low-cost magnetic, angular rate and gravity systems. *Sensors* **2015**, *15*, 25919–25936. [[CrossRef](#)] [[PubMed](#)]
18. Ren, C.H.; Liu, Q.Q.; Fu, T.D. A novel self-calibration method for MIMU. *IEEE Sens. J.* **2015**, *15*, 5416–5422. [[CrossRef](#)]
19. Zhang, Z.Q. Two-step calibration methods for miniature inertial and magnetic sensor units. *IEEE Trans. Ind. Electron.* **2015**, *62*, 3714–3723. [[CrossRef](#)]
20. Schopp, P.; Graf, H.; Burgard, W. Self-calibration of accelerometer arrays. *IEEE Trans. Instrum. Meas.* **2016**, *65*, 1913–1925. [[CrossRef](#)]
21. Yadav, N.; Bleakley, C. Fast calibration of a 9-DOF IMU using a 3 DOF position tracker and a semi-random motion sequence. *Measurement* **2016**, *90*, 192–198. [[CrossRef](#)]



© 2017 by the authors. Licensee MDPI, Basel, Switzerland. This article is an open access article distributed under the terms and conditions of the Creative Commons Attribution (CC BY) license (<http://creativecommons.org/licenses/by/4.0/>).